Available online at www.sciencedirect.com
SCIENCE DIRECT®
Estuarine, Coastal and Shelf Science 57 (2003) 715–724
ESTUARINE COASTAL AND SHELF SCIENCE

Modelling eutrophication in mesotidal and macrotidal estuaries. The role of intertidal seaweeds

A. Alvera-Azcárate[a], J.G. Ferreira[b,*], J.P. Nunes[b]

[a]*G.H.E.R.—GeoHydrodynamics and Environment Research—Sart Tilman, Université de Liège, 4000 Liège, Belgium*
[b]*IMAR—Institute of Marine Research, Centre for Ecological Modelling, DCEA-FCT, Qta. Torre, 2825-114 Monte de Caparica, Portugal*

Received 12 June 2002; accepted 18 November 2002

Abstract

The role of intertidal seaweeds in the primary production of mesotidal and macrotidal estuaries has been examined by means of a model, applied to the Tagus Estuary (Portugal). Special attention was paid to the description of the underwater light climate in intertidal areas, and to the importance of the formation of tidal pools. Two approaches were compared for the simulation of suspended particulate matter (SPM) in the pool areas, using three algal species.

The use of an erosion–deposition approach to simulate the distribution of SPM in tidal pools gives an increase in net primary productivity per unit area of between 130 and 1300%, when compared to the more conventional approach where the suspended matter in the overlying water in intertidal areas is considered identical to that in the channels.

The upscaled erosion–deposition model was applied to tidal pool areas and combined with the more conventional model for other intertidal areas. Results show that annual carbon fixation by intertidal seaweeds in the estuary exceeds 13,500 t C yr^{-1}, and accounts for 21% of the total carbon fixed by all primary producers. The corresponding nitrogen removal by seaweeds corresponds to the annual nutrient loading of a population of 490,000 inhabitants.

Keywords: seaweeds; model; eutrophication; mass balance; Tagus Estuary

1. Introduction

Increased pressures on estuarine and coastal ecosystems have resulted in progressively greater nutrient inputs, leading to the occurrence of eutrophication (e.g. Gustafson, Fleischer, & Joelsson, 2000; Lohrenz et al., 1999; Stapleton, Kay, Jackson, & Wyer, 2000). Primary producers remove a large part of these nutrients from the ecosystem (Gao & McKinley, 1994; Herbert, 1999; NICE, 1999), and in the process, important changes to ecosystem structure may occur. These changes, which have been classified as primary and secondary eutrophication symptoms by Bricker, Clement, Pirhalla, Orlando, and Farrow (1999) manifest themselves, for instance, in the increased turbidity of the water column, due to elevated phytoplankton concentrations, which reduces light availability to benthic primary producers, and in the disappearance of seagrasses. Seaweeds, in particular fast-growing opportunistic genera such as *Ulva* and *Enteromorpha*, may replace other benthic vegetation and form algal mats, leading to strong oscillations in dissolved oxygen, and to the development of substantial amounts of organic detritus (e.g. Boesch, 2002; Flindt et al., 1997).

The high turbidity of mesotidal and macrotidal estuaries along the European Atlantic seaboard, resulting from strong tidal currents and bottom resuspension of fine particulates, may naturally limit phytoplankton growth (e.g. Gianesella, Saldanha-Correa, & Teixeira, 2000; Muylaert & Sabbe, 1999). In this type of system, light is a key limiting factor for pelagic primary production (Cloern, 1999). Furthermore, the phytoplankton component of suspended particulate matter (SPM) will account for only a small percentage of the total

* Corresponding author.
E-mail address: joao.imar@mail.telepac.pt (J.G. Ferreira).

0272-7714/03/$ - see front matter © 2003 Elsevier Science B.V. All rights reserved.
doi:10.1016/S0272-7714(02)00413-4

mass, and will not be a major determinant of turbidity: e.g. a 20 mg m^{-3} concentration of chlorophyll *a* (chl *a*) corresponds to only 4–7% of a SPM concentration of 50 mg l^{-1} (using a range of carbon: chl *a* ratios of 35–60). Estuaries with a high tidal range usually have large tidal flat areas, and sizeable natural macrophytobenthic communities, which play an important role in carbon fixation and nutrient removal in shallow waters (Ferreira & Ramos, 1989; Gao & McKinley, 1994; Simas, Nunes, & Ferreira, 2001). Sub-tidal benthic primary production will probably not have much expression due to natural turbidity.

The significance of this partitioning of primary production is twofold: (i) increased nutrient loading will probably not result in increased phytoplankton concentrations, but may result in pelagic species shifts, including the appearance of harmful or toxic algae; and (ii) benthic primary producers, especially those associated with intertidal areas (seaweeds, microphytobenthos) and the upper limits of the tidal range (saltmarsh vegetation), will show increased productivity, acting as a bioremediation mechanism for eutrophication (CCME, 2000; Herbert, 1999).

There has only been a limited amount of work in estimating seaweed production in mesotidal estuaries, either using cropping methods (e.g. Murthy, Ramakrishna, Sarat Babu, & Rao, 1986) which are notoriously error-prone, or through the application of simple models based on dynamic production measurements and estimates of areal coverage (e.g. Ferreira & Ramos, 1989). Benthic primary productivity in shallow waters is strongly dependent on the regulation of underwater light climate by SPM (Herbert, 1999; Lohrenz et al., 1999; Schild & Prochnow, 2001)—if an excess of nutrients exists, light availability will be the key limitation. In intertidal areas, the combination of shallow waters and strong tidal currents creates a complex pattern of SPM transport, deposition, and resuspension dynamics (e.g. Portela & Neves, 1994; Van Wijngaarden, 1999). The formation of isolated water pools on tidal flats at low tide, where SPM deposits in a few minutes, increases the complexity of these dynamics.

In ecological models, the concentration of SPM in intertidal areas has previously been simulated by using values for the main flow channels (e.g. Baretta & Ruardij, 1988; Ferreira, Duarte, & Ball, 1997) or simply by correlating with tidal amplitude (Black, 1998; Ferreira & Ramos, 1989; Periañez, Abril, & Garcia-Leon, 1996; Simas et al., 2001). A more accurate representation of sediment dynamics is the direct calculation of the shear stress exerted by water current on the sediment, causing resuspension or deposition (Portela & Neves, 1994; Schild & Prochnow, 2001; Van Rijn, 1993; Van Wijngaarden, 1999).

An improved simulation of the dynamics of SPM appears to be a key factor in determining the role of benthic primary production in estuarine nutrient dynamics, and therefore in the potential development of eutrophication symptoms. The main objective of this study was to develop a more mechanistic approach to modelling of seaweed productivity, by improving the description of the underwater light climate in intertidal areas over the whole tidal cycle, accounting for the formation of tide pools, and upscaling the benthic productivity model in space (to the whole system) and time (for an annual cycle). The model has been applied and tested in a large mesotidal system (Tagus Estuary—Portugal), by combining field and experimental data, small spatial scale modelling, and geographical information systems (GIS). Results at the system scale obtained using this approach are compared with those from a more classical formulation of SPM dynamics based on correlation with tidal amplitude.

2. Methods

2.1. Site description

The Tagus Estuary in Portugal (Fig. 1) was chosen as a test site for the modelling work, for the following reasons:

(1) The estuary is a large (320 km^2) mesotidal system (mean tidal range: 2.2 m) with an intertidal area of about 130 km^2 (Ferreira & Ramos, 1989; Simas et al., 2001), and receives a modal freshwater inflow of 400 $m^3 s^{-1}$. The system is vertically well-mixed, and has a mean tidal prism of 600×10^6 m^3, about a third of the mean volume (Carvalho, Ferreira, Amorim, Marques, & Ramos, 1997). Turbidity depends mainly on tidal amplitude (Fig. 2) and SPM concentrations are higher at low tide than high tide. The mean solid load from the Tagus River is about 400×10^3 t yr^{-1}; in the estuary, mean SPM concentrations range from 20 mg l^{-1} in a neap tide to 140 mg l^{-1} in a spring tide, although in spring tides the maximum turbidity zone has SPM concentrations of up to 350 mg l^{-1} (Martins & Düffner, 1982). Channels and pools are formed in intertidal areas during the ebb, and persist for a part of the tidal cycle. In these pools, SPM sediments quickly, with the water becoming clear after a few minutes; SPM resuspends with the rising tide and water exchange with the main channels occurs.

(2) Benthic photosynthetic organisms account for an estimated 27% of the total primary production (Ferreira & Ramos, 1989; Serôdio & Catarino, 2000; Simas et al., 2001). The distribution of the dominant seaweed species is zoned by depth: *Fucus vesiculosus* (1.2 m above tidal datum, often emerged), *Ulva lactuca* (1 m), and *Gracilaria verrucosa* (0.8 m, almost always immersed).

(3) The estuary receives a nutrient input corresponding to about 3×10^6 population equivalents (PEQ), resulting from domestic and industrial discharges (Ferreira, 2000).

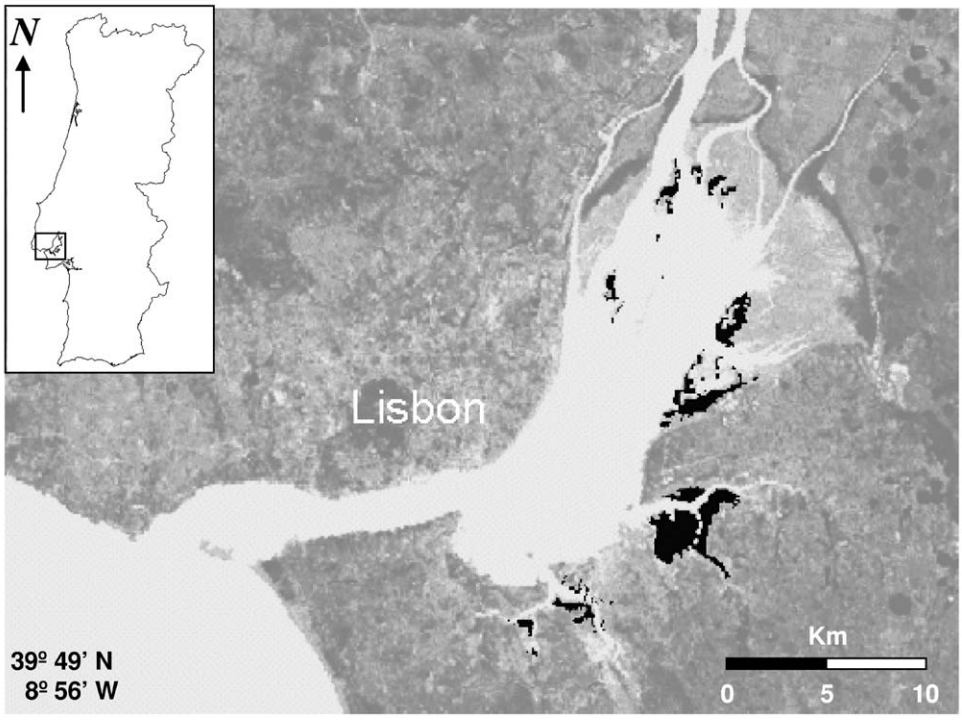

Fig. 1. The Tagus Estuary (Portugal). Seaweed areas are shown in black (Crespo, personal communication).

2.2. Model development

2.2.1. Seaweed model

Table 1 presents the main equations and parameters used for the macroalgal model. Eq. (1) was used to calculate biomass variation, which depends on gross production and respiration. Gross production was simulated by combining the maximum production P_{max} (Eq. (2)) with a hyperbolic function for light energy at the surface of the macroalgae (Eq. (3)). A light saturation function was selected because seaweeds do not normally exhibit photoinhibition, or are only photoinhibited at very high light intensity (Hanelt, Melchersmann, Wiencke, & Nultsch, 1997; Valiela, 1995). Losses by respiration were considered to be about 10% of

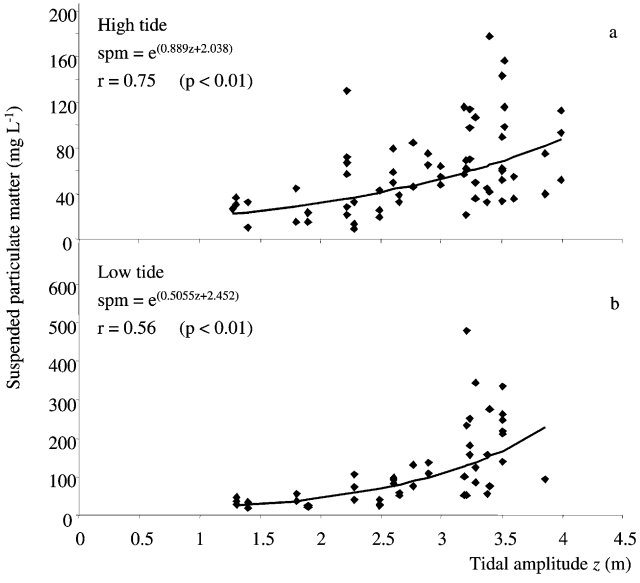

Fig. 2. Relationship between SPM and tidal amplitude for high water (a) and low water (b), showing the regression lines and equations.

Table 1
Main equations used for the seaweed model

Model equations		Comments
$\frac{dB}{dt} = B(P_g - R)$	(1)	R values for the three simulated macroalgae (Ferreira & Ramos, 1989):
B—seaweed biomass (expressed as C)		*Fucus vesiculosus* (0.0875)
t—time		*Ulva lactuca* (0.27)
P_g—seaweed gross production rate ($mg\,C\,g\,dw^{-1}\,h^{-1}$)		*Gracilaria verrucosa* (0.372)
R—seaweed respiration rate ($mg\,C\,g\,dw^{-1}\,h^{-1}$)		
$P_g = P_{max} f(I)$	(2)	P_{max} values for three simulated macroalgae (Ferreira & Ramos, 1989):
$f(I) = \frac{I}{I_k + I}$	(3)	*Fucus vesiculosus* (0.83)
P_{max}—maximum gross production rate ($mg\,C\,g\,dw^{-1}\,h^{-1}$)		*Ulva lactuca* (2.32)
$f(I)$—hyperbolic light intensity function		*Gracilaria verrucosa* (3.12)
I—light intensity ($W\,m^{-2}$)		
I_k—half-saturation constant for I		

the total production (Ferreira & Ramos, 1989). As a first approach, respiration losses were considered to be associated only with the production processes. Nutrients were not included in the model, since it has been shown that primary production in this ecosystem is limited by light availability (e.g. Macedo, Ferreira, & Duarte, 1998; Serôdio & Catarino, 2000). However, the model may be generalized very easily by including nutrient limitation.

2.2.2. Light climate

Light energy available at the water surface I_0 ($W\,m^{-2}$) was calculated according to Brock (1981), considering the annual light energy variation, the photoperiod, and the photosynthetically active radiation (PAR). Attenuation in the water column by SPM absorption, parametrized by the extinction coefficient k (m^{-1}), results in I_z ($W\,m^{-2}$) the light intensity at the depth $z(t)$, calculated from the Lambert–Beer equation:

$$I_z = I_0\, e^{-kz} \tag{4}$$

The depth z is different for each seaweed species, because zonation depends on bathymetry and resistance to emersion. The light extinction coefficient depends linearly on the SPM (Fig. 3). The relationship was obtained from the BarcaWin2000™ water quality database, using SPM and k data obtained from 17 different stations of the Tagus Estuary.

2.2.3. Tide and velocity simulation

In mesotidal and macrotidal estuaries, tides establish the regime of emersion–immersion periods for intertidal species, and are a key determinant of the hydrodynamics. The basic harmonic constituents were used to simulate tidal height and time, from a specific origin in time (January 1, 1980). The water velocity u was simulated as a sinusoidal function:

$$u = A\sin(vt + p) \tag{5}$$

where A (m) is the amplitude of the water current and v ($m\,s^{-1}$) is the wave velocity. Considering that the dynamics of the intertidal zones are mainly affected by tides, the water velocity was calculated by considering the time between a low tide and a high tide, and the distance covered in this period, determining the current velocity, and thus the distance covered by water during the flood and ebb. Fig. 4 shows how velocity varied with respect to the tide: the velocity was considered zero at high and low water, and reaches maximum values at mid-tide.

2.2.4. Sediment dynamics

Because of the strong tidal currents in mesotidal and macrotidal estuaries, phytoplankton may not play a major role in water turbidity, when compared to SPM (e.g. Gianesella et al., 2000; Muylaert & Sabbe, 1999), which therefore becomes the most important factor affecting the light climate below the surface. Two alternative methods for simulating the SPM concentration in the water column were applied herein, and are briefly described below. The parameters for the model equations are shown in Table 2.

2.2.4.1. The 'interpolation' method. Several studies (Black, 1998; Ferreira & Ramos, 1989; Periañez et al., 1996; Simas et al., 2001) indicate that there is a close relationship between the tidal range and the mass of suspended sediments in the water. Data for an upstream sampling station situated near the tidal flats were used to derive relationships for high (Fig. 2a) and low (Fig. 2b) tide conditions, which were then used to obtain the SPM concentration. A simple interpolation was used at each timestep (Eq. (6)) based on the high water and low water SPM concentrations.

$$\mathrm{SPM}_t = \frac{z_t - z_{\min}}{z_{\max} - z_{\min}}\mathrm{SPM}_{\mathrm{lw}} + \frac{z_{\max} - z_t}{z_{\max} - z_{\min}}\mathrm{SPM}_{\mathrm{hw}} \tag{6}$$

where SPM_t is suspended particulate matter at time t; $\mathrm{SPM}_{\mathrm{hw}}$ and $\mathrm{SPM}_{\mathrm{lw}}$ are SPM concentrations for high water and low water conditions, respectively; z_t is tidal height at time t; and $z_{\max}$ and $z_{\min}$ are high water and low water depths, respectively.

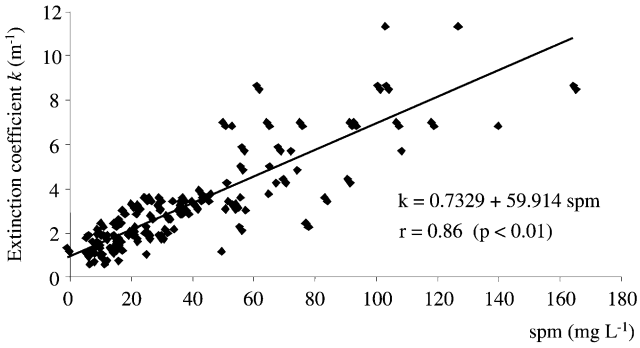

Fig. 3. Extinction coefficient as a function of SPM showing the regression line and equation.

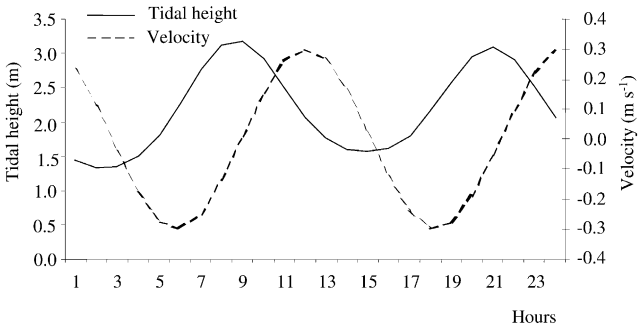

Fig. 4. Velocity variation with tidal height over a tidal cycle.

Table 2
Parameters used for the SPM models

Symbol	Units	Meaning	Value	Reference
ρ_p	$kg\,m^{-3}$	Particle density	2650	Quintela (1985)
ρ_w	$kg\,m^{-3}$	Water density	998	White (1986)
N	$s\,m^{-1/3}$	Manning's roughness coefficient	0.014	Lencastre and Franco (1992)
μ	$N\,m\,s^{-1}$	Water viscosity	0.1003×10^{-2}	White (1986)
R	M	Particle ratio	1×10^{-5}	http://www.science.ubc.ca
g	$m\,s^{-2}$	Acceleration of gravity	9.81	–
τ_d	$N\,m^{-2}$	Critical shear stress for deposition	0.35	Berlamont, Ockenden, Toorman, and Winterwerp (1993), Cole and Miles (1983), Lobmeyr, Kappenberg, and Grabemann (1993), and Van Rijn (1993)
τ_e	$N\,m^{-2}$	Critical shear stress for erosion	0.3	Cole and Miles (1983)
M	$kg\,m^{-2}\,s^{-1}$	Erosion rate coefficient	12×10^{-5}	Portela and Neves (1994)
A	M	Amplitude of the water current wave	0.3	–

In this approach, the SPM concentration varies as a function of the tidal height variation, which remains constant when tidal pools are formed. Since during this period there was no change in water height, SPM also remains unchanged.

2.2.4.2. The 'erosion–deposition' method. The sediment modelling approach may be improved by accounting for the sediment dynamics of tidal pools. In the 'interpolation method', the SPM concentration changes only with water height, and the effect of tidal currents on SPM during the formation of tidal pools is ignored. The shear stress exerted over the bottom sediments depends mainly on water velocity and tidal height, and defines the rates of sediment erosion and deposition. At high water velocities sediment resuspension increases and vertical turbulence prevents settling; during tidal pool formation, sediments deposit rapidly. This was modelled using erosion–deposition formulations, after Portela and Neves (1994), Periañez et al. (1996), Schild and Prochnow (2001), Van Rijn (1993), and Van Wijngaarden (1999).

2.2.4.2.1. Deposition. Deposition D ($kg\,m^{-2}\,s^{-1}$) is given by Krone's equation (Krone, 1962):

$$D = \begin{cases} w_{fall}\mathrm{SPM}\left(1 - \left(\frac{\tau}{\tau_d}\right)\right) & \text{if } \tau \le \tau_d \\ 0 & \text{if } \tau > \tau_d \end{cases} \quad (7)$$

To describe the deposition rate it is necessary to account for the fall velocity of particles, w_{fall} ($m\,s^{-1}$), using Stokes' law:

$$w_{fall} = \frac{2}{9} g \frac{(\rho_p - \rho_w)}{\mu} r^2 \quad (8)$$

where ρ_w and ρ_p ($kg\,m^{-3}$) are the water and particle density, g is the acceleration of gravity ($m\,s^{-2}$), μ is the water viscosity ($N\,m\,s^{-1}$) and r is the particle radius (m).

τ_d ($N\,m^{-2}$) is the critical shear stress and τ ($N\,m^{-2}$) is the bed-shear stress, expressed by:

$$\tau = \rho_p c_b u^2 \quad (9)$$

where u ($m\,s^{-1}$) is the water velocity, and c_b (adimensional) is a bed-shear coefficient (Eq. (10)):

$$c_b = \frac{g n^2}{h^{1/3}} \quad (10)$$

where n ($s\,m^{-1/3}$) is the Manning roughness coefficient and h (m) is the water column depth. When the bed-shear stress τ falls below the critical value, τ_d, deposition occurs and particles deposit at a w_{fall} speed.

2.2.4.2.2. Erosion. The erosion rate, E ($kg\,m^{-2}\,s^{-1}$) was calculated after Partheniades (1965):

$$E = \begin{cases} M\left(\frac{\tau}{\tau_e} - 1\right) & \text{if } \tau \ge \tau_e \\ 0 & \text{if } \tau < \tau_e \end{cases} \quad (11)$$

where M ($kg\,m^{-2}\,s^{-1}$) is the erosion rate coefficient and τ_e ($N\,m^{-2}$) is the critical shear stress for erosion. Erosion occurs when the bed-shear stress is greater than the critical value.

2.2.4.2.3. Formation of tidal pools. On the ebb, tidal pools are formed. Neglecting the wind, the water velocity in pools during this period is considered to be zero, as they are disconnected from the channels, so the bed-shear stress τ will also be zero. Under these conditions, deposition and erosion are different and must be treated separately from the rest of the tidal cycle.

Deposition is maximal, because there is no water turbulence preventing particles from sinking, i.e. the condition $\tau \le \tau_d$ is always true, and may be described by:

$$D = w_{fall}\mathrm{SPM} \quad (12)$$

Conversely, bottom erosion is zero, because there is no bed-shear stress, and the condition $\tau > \tau_e$ is always true.

Tidal pools are formed only in a small interval of the tidal cycle. They are disconnected from the main system of currents for a few hours, but this is sufficient to cause a very rapid deposition of the particles suspended in the

water. Depending on the tidal height at which tidal pools are formed, the algae that colonize higher regions are exposed (e.g. *F. vesiculosus*) while other species remain immersed over the entire cycle.

2.2.4.2.4. Suspended particulate matter. Erosion (E) and deposition (D) depend on the water velocity, deposition rate also depends on the total SPM in the water column, and the value of SPM was recalculated at each time step:

$$\frac{\mathrm{dSPM}}{\mathrm{d}t} = E - D \tag{13}$$

2.2.5. Simulations

Seaweed productivity was simulated over a period of 1 yr at the scale of 1 m^2, using three different depths (one for each seaweed species) and the two different SPM formulations described above. An initial condition of 60 mg l^{-1} SPM (Portela and Neves, 1994) was used for the SPM modelling, and the models were run with a 1-min timestep for hydrodynamics and SPM and an hourly timestep for light climate and productivity. Since the model does not include other processes which affect the biomass of seaweeds, such as erosion losses or grazing, the simulation was run operationally, by monthly reinitializing the areal biomass for each species based on measured data from Ferreira and Ramos (1989). It takes a few minutes to run the model for 1 yr.

2.2.6. Upscaling

The results were obtained at the scale of 1 m^2, and subsequently upscaled to the whole system, using remote sensing and GIS. To upscale the results, the bathymetry was superimposed on a substrate map taken from a SPOT satellite image (Crespo, personal communication). The depth distribution of the seaweed areas shows a large area at 1.5 m above datum, occupied primarily by *F. vesiculosus* and also to some extent by *U. lactuca*. The middle zones are colonized by *U. lactuca*, and the deeper zones by *G. verrucosa*.

The seaweed species considered for the model occupy an area of 16.5 km^2 (Fig. 1) with 36% coverage of *F. vesiculosus*, 46% of *U. lactuca*, and 18% of *G. verrucosa*. (Ferreira & Ramos, 1989). Based on a heuristic assessment, 50% of this area is considered to be occupied by tidal pools. In order to compare the overall results for the two modelling approaches, the model was run considering the following conditions:

(a) The 'interpolation' model was upscaled over the whole area of 16.5 km^2.
(b) The 'erosion–deposition' model was upscaled over 50% of this area, corresponding to tidal pools, and the remaining area was upscaled with the 'interpolation' model. The two results were combined to determine the overall production.

2.2.7. Model implementation

The modelling system was developed in Borland C++ Builder 5™ (BCB), using object-oriented programming. BCB allows for a rapid implementation of a sophisticated interface which promotes usability, taking advantage of a range of ActiveX components for spreadsheet-based data input and output, and graphical and file outputs.

3. Results

3.1. Sediment dynamics and tide pool formation

Sediment dynamics vary greatly when calculated using the interpolation (Fig. 5a) and erosion–deposition (Fig. 5b) models. In the former model, SPM values show a minimum at high tide and a maximum at low tide. Tidal pool formation is shown schematically in Fig. 5. In the interpolation model, pools are formed when tidal height drops below 1.2 m, but SPM does not deposit. The more realistic erosion–deposition model shows smaller values of SPM when tide pools are formed, due to the complete sedimentation of SPM (Fig. 5b). During the flood, the current induces resuspension of bottom sediment and increases the SPM concentration in the water column. If the two models are run over longer time scales (e.g. a month) the average SPM concentration obtained with the erosion–deposition approach is significantly lower (e.g. January data: 19 mg l^{-1} compared to 40 mg l^{-1} for the interpolation method).

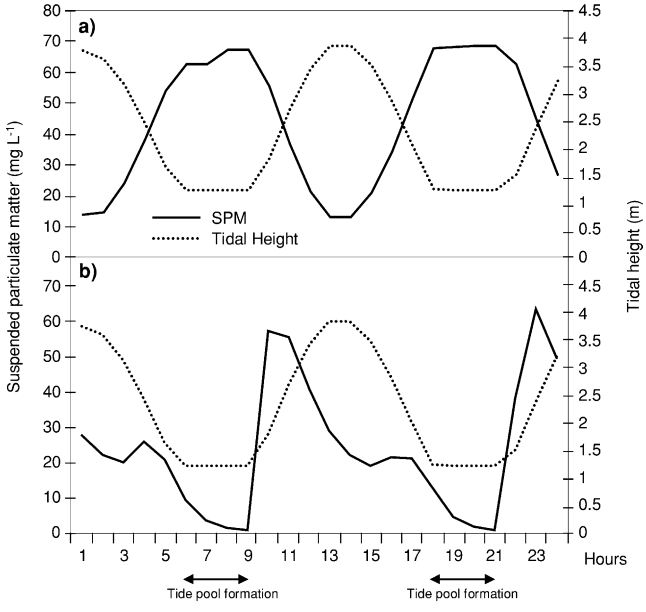

Fig. 5. Variation of SPM and tidal height over a tidal cycle, using the interpolation (a) and erosion–deposition (b) models.

The tidal height at which tidal pools are formed varies, and this affects mainly species such as *F. vesiculosus*. If this tidal height were above 1.2 m, these algae would be covered by water, but if it is lower, the algae are exposed for a few hours each tidal cycle. It is unclear from the literature whether production stops completely during exposure, or continues while the seaweeds are not dessicated, particularly since the nutrient supply may follow a cell-quota model. However, since there is considerable uncertainty regarding rates, and since emerged production is not forced by SPM, seaweed production is considered to stop during periods of exposure to the atmosphere.

Fig. 6 shows seaweed production over a tidal cycle, during which a tidal pool is formed at a depth of 1.2 m above datum. Species colonizing the higher intertidal zone (e.g. *F. vesiculosus*) remain exposed, and their production decreases to zero; other species of macroalgae, which occupy the lower areas, remain immersed in the tidal pools formed over the low tide period, and have high production rates—the water column depth (and optical path) is small, SPM sharply decreases, so the light climate is at an optimum.

As tidal pool formation occurs frequently in mesotidal and macrotidal estuaries, its effects—SPM deposition and algal emersion—are important. The proportion of the intertidal area which forms pools at low tide, and the distribution of pool depths are difficult to determine, requiring detailed bathymetric data. For the present simulations, 50% of the total intertidal area is considered to form pools during low tide, located below the 1.2 m height level, and with a depth varying with the local bathymetry (average pool depth = 20 cm). This reflects the normal situation, where *F. vesiculosus* is exposed at mean low tide and other species remain underwater.

3.2. Primary production

The results of the annual gross primary production (GPP) and net primary production (NPP) per unit area obtained with each model are shown in Table 3. For all species, the erosion–deposition approach gives much higher annual productivities than the interpolation model, due to the improved simulation of the underwater light climate. For NPP, the increase is 128% for *F. vesiculosus*, 240% for *U. lactuca*, and 1317% for *G. verrucosa*, i.e. the species which colonize the deeper parts of the intertidal zone show the largest increases, due to the reduced light attenuation over a greater optical path. Additionally, it can be seen that the green seaweed *U. lactuca*, which is the most productive of the three using the interpolation model (6% more than *Fucus*) becomes 60% more productive than *Fucus* using the erosion–deposition model. This would be expected in fast-growing opportunistic seaweeds such as *Ulva* or *Enteromorpha*. The relative role of the more sub-tidal species in overall seaweed production also increases dramatically: *Gracilaria* shows a 1300% increase in NPP between the two models, and reaches a similar annual production to *F. vesiculosus*, of about 600 gC $m^{-2} yr^{-1}$.

The erosion–deposition and the interpolation model results were combined to calculate turnover rates for each seaweed (Table 3). The fast-growing green algae have a turnover of 18 yr^{-1}, due to a high productivity and capacity to colonize new substrates, and the red seaweeds have even greater turnover, although production is much lower than for *Ulva*. *Fucus* shows a relatively low turnover of about 4 yr^{1}. These values are higher than previously reported (Ferreira & Ramos, 1989), particularly for the green and red algae. This would be expected from the improved simulation approach, and will potentially allow a better description of benthic eutrophication events.

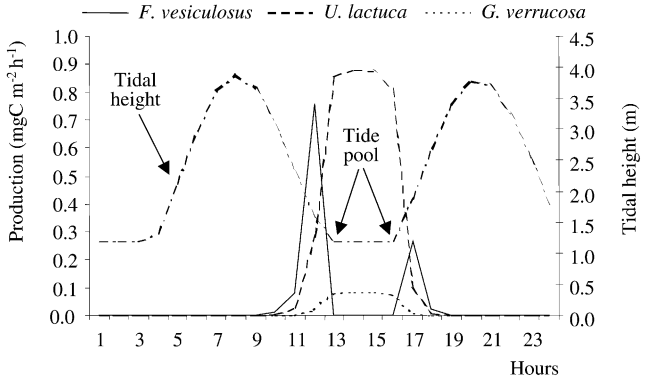

Fig. 6. Seaweed production in an intertidal area over a tidal cycle. Tide pool formation occurs at 1.2 m above tidal datum.

3.3. Carbon and nitrogen budgets

In order to estimate the role of seaweeds in annual estuarine carbon and nitrogen budgets, the two small-scale primary productivity models were combined to

Table 3
Mean annual biomass, annual GPP and NPP for both models and turnover rate for each species calculated using the combined erosion–deposition model (tidal pools) and interpolation model (other areas)

Seaweed species	*Fucus vesiculosus*	*Ulva lactuca*	*Gracilaria verrucosa*
Mean biomass[a] (gC m^{-2})	199	59	27
Interpolation model			
GPP (gC $m^{-2} yr^{-1}$)	531	609	211
NPP (gC $m^{-2} yr^{-1}$)	286	305	42
Erosion–deposition model			
GPP (gC $m^{-2} yr^{-1}$)	918	1460	896
NPP (gC $m^{-2} yr^{-1}$)	654	1038	601
Turnover P/B (yr^{-1})	4	18	21

[a] Data from Ferreira and Ramos (1989) based on monthly measurements over a 2-yr period.

determine the productivity for the whole system (Fig. 7)—as described earlier, 50% of the area (tidal pool) using the erosion–deposition model and 50% (other areas) using the interpolation model. Previous estimates of GPP of 5077 t C yr^{-1}, obtained by Ferreira and Ramos (1989), are lower than the 8390 t C yr^{-1} obtained with the interpolation method in this work. Furthermore, when the combined interpolation and erosion–deposition approach is used, productivity estimates are substantially higher: the seaweed GPP is 13,770 t C yr^{-1} and the NPP is 8820 t C yr^{-1}.

The modelling approaches used herein do not, however, incorporate: (a) grazing, which will lower the productive biomass; (b) mortality and erosion, which will also reduce biomass; and (c) wind effects, which may cause some resuspension in tidal pools even when the intertidal areas are decoupled from the main estuarine channels. The first two factors are partly compensated by the fact that this is an operational model, with monthly reinitialization of seaweed biomasses.

Based on the results obtained with the erosion–deposition model, a comparative analysis of the role of different primary producers may be carried out (Table 4). Phytoplankton accounts for about 62% of total primary production, while benthic primary producers are responsible for 38% of carbon fixation (about 25,700 t C yr^{-1}).

If NPP is considered, seaweeds annually fix about 8800 t of carbon, which becomes potentially available to higher trophic levels—considering three trophic levels and an ecological efficiency of 0.1, this would correspond to about 2600 t of fish (fresh weight).

When the GPP results are applied to nitrogen removal, the overall nitrogen uptake corresponding to an annual production of 67 kt of carbon, using a Redfield C : N ratio of 45 : 7 in mass, and a PEQ of 4.4 kg N yr^{-1}, is about 10.5 kt N yr^{-1}, equivalent to 2.3×10^6 inhabitants, which exceeds the population on the estuarine perimeter by about 15%.

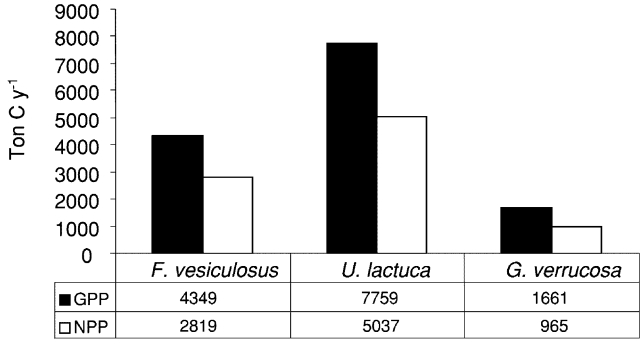

Fig. 7. Total annual seaweed production for the Tagus Estuary, estimated with the combined erosion–deposition model (tidal pools) and interpolation model (other areas).

Table 4
Contribution by pelagic and benthic primary producers to the Tagus Estuary carbon budget (all values in t C yr^{-1})

Pelagic producers			Benthic producers		
Phytoplankton[a]	41,160	62%	Microphytobenthos[b]	4265	6%
			Seaweeds[c]	13,770	21%
			Saltmarsh vegetation[d]	7700	11%
Sub-total pelagic	41,160	62%	Sub-total benthic	25,735	38%
Total GPP			66,895 t C yr^{-1}		

[a] EcoWin2000 ecological model, Ferreira (2000).
[b] Modelling and field measurements, Serôdio and Catarino (2000).
[c] This work, using the combined erosion–deposition model for tidal pools and interpolation model for other areas.
[d] Modelling and field measurements, Simas et al. (2001).

4. Discussion

The methodology developed in this work is focussed on accurately simulating the underwater light climate, by considering water turbidity as a key factor in the light field variation, and also the special conditions of water clarity which occur at low tide, when tidal pools are formed. The tidal cycle is a key factor, particularly if nutrient limitation is not critical, and seaweed production is essentially constrained by light and emersion.

The role of benthic autotrophs in cycling carbon and nutrients is often less well recognized than that of the pelagic component, but it is apparent from these results that in mesotidal or macrotidal turbid estuaries it may be as important. The application of our combined model indicates that from seaweeds alone, nitrogen removal may be equivalent to the loading of about 490,000 people, which shows that seaweeds may play a significant buffer role in maintaining nitrogen balance.

In this type of estuary, where turbidity depends mainly on SPM resuspension rather than on phytoplankton, increased nutrient loading may not result in the loss of submerged (subtidal) aquatic vegetation, or in increased phytoplankton blooms, given the role of light as a limiting factor for pelagic production. Changes are more likely to be manifested as a shift in phytoplankton species composition, including the appearance of harmful or toxic species, and in alterations to benthic primary production.

In particular, enhanced seaweed production in the intertidal zone is one of the key potential symptoms of eutrophication, which highlights the importance of an accurate description of annual production. The erosion–deposition model applied in this work has shown that estimates of carbon fixation and nutrient removal, using uniform SPM dynamics for the whole system, may significantly underestimate the role of intertidal seaweeds, and have important consequences for

the understanding of carbon and nitrogen cycling in mesotidal and macrotidal estuaries.

Acknowledgements

The authors are grateful to the Eurosam (EU-DG XII) and Festa II (FCT) projects for funding parts of this work, and to L. Portela for help on sediment dynamics. Helpful comments by two anonymous reviewers are also acknowledged.

References

Baretta, J., & Ruardij, P. (Eds.). (1988). *Tidal flat estuaries. Simulation and analysis of the Ems Estuary* (70 pp.). Berlin: Springer.

Berlamont, J., Ockenden, M., Toorman, E., & Winterwerp, J. (1993). The characterisation of cohesive sediment properties. *Coastal Engineering 21*, 105–128.

Black, S. K. (1998). Suspended sediment dynamics and bed erosion in the High Shore Mudflat region of the Humber Estuary. *Marine Pollution Bulletin 37*, 122–133.

Boesch, D. (2002). Challenges and opportunities for science in reducing nutrient over-enrichment of coastal ecosystems. *Estuaries 25*, 744–758.

Bricker, S. B., Clement, C. G., Pirhalla, D. E., Orlando, S. P., & Farrow, D. R. G. (1999). National estuarine eutrophication assessment: Effects of nutrient enrichment in the nation's estuaries. (71 pp.). Silver Spring, MD: NOAA, National Ocean Service, Special Projects Office and the National Centers for Coastal Ocean Science.

Brock, T. D. (1981). Calculating solar radiation for ecological studies. *Ecological Modelling 14*, 1–19.

Carvalho, M. L., Ferreira, J. G., Amorim, P., Marques, M. I. M., & Ramos, M. T. (1997). Study of heavy metals and other elements in macrophyte algae using energy-dispersive X-ray fluorescence. *Environmental Toxicology and Chemistry 16*, 807–812.

Cloern, J. E. (1999). The relative importance of light and nutrient limitation of phytoplankton growth: a simple index of coastal ecosystem sensitivity to nutrient enrichment. *Aquatic Ecology 33*, 3–16.

Cole, P., & Miles, G. V. (1983). Two-dimensional model of mud transport. *Journal of Hydraulic Engineering 109*, 1–12.

Committee on the Causes and Management of Eutrophication (CCME), Ocean Studies Board, Water Science and Technology Board, National Research Council (2000). Clean coastal waters: Understanding and reducing the effects of nutrient pollution (428 pp.). Washington, DC: National Academy Press.

Ferreira, J. G. (2000). Development of an estuarine quality index based on key physical and biogeochemical features. *Ocean and Coastal Management 43*, 99–122.

Ferreira, J. G., Duarte, P., & Ball, B. (1997). Trophic capacity of Carlingford Lough for aquaculture—analysis by ecological modelling. *Aquatic Ecology 31*, 361–378.

Ferreira, J. G., & Ramos, L. (1989). A model for the estimation of annual production rates of macrophyte algae. *Aquatic Botany 33*, 53–70.

Flindt, M. R., Kamp-Nielsen, L., Marques, J. C., Pardal, M. A., Bocci, M., Bendoricchio, G., Nielsen, S. N., & Jørgensen, S. E. (1997). Description and comparison of three shallow estuaries: Mondego River (Portugal), Roskilde Fjord (Denmark) and the Lagoon of Venice (Italy). *Ecological Modelling 102*, 17–31.

Gao, K., & McKinley, K. R. (1994). Use of macroalgae for marine biomass production and CO_2 remediation: a review. *Journal of Applied Phycology 6*, 45–60.

Gianesella, S. M. F., Saldanha-Correa, F. M. P., & Teixeira, C. (2000). Tidal effects on nutrients and phytoplankton distribution in Bertioga Channel, Sao Paulo, Brazil. *Aquatic Ecosystem Health and Management 3*, 533–544.

Gustafson, A., Fleischer, S., & Joelsson, A. (2000). A catchment-oriented and cost-effective policy for water protection. *Ecological Engineering 14*, 419–427.

Hanelt, D., Melchersmann, B., Wiencke, C., & Nultsch, W. (1997). Effects of light stress on photosynthesis of polar macroalgae; relation to depth distribution. *Marine Ecology Progress Series 149*, 255–266.

Herbert, R. A. (1999). Nitrogen cycling in coastal marine ecosystems. *FEMS Microbiology Reviews 23*, 563–590.

Krone, R. B. (1962). *Flume studies of the transport of sediment in estuarial shoaling processes* (pp. 1–118). Final Report, Hydraulic Engineering Laboratory and Sanitary Engineering Research Laboratory, Berkeley, CA (prepared for US Army Engineer District, San Francisco, San Francisco, CA, under US Army Contract No. DA-04-203 CIVENG-59-2).

Lencastre, A., & Franco, F. M. (1992). *Lições de hidrologia* (2nd ed., 453 pp.). Lisbon: New University of Lisbon (in Portuguese).

Lobmeyr, M., Kappenberg, J., & Grabemann, I. (1993). Modelling of sediment dynamics in the harbour area of Bremen. In L. C. Wrobel & C. A. Brebbia (Eds.), *Water pollution II, modelling, measuring and prediction* (pp. 217–224). Southampton: CMP.

Lohrenz, S. E., Fahnenstiel, G. L., Redalje, D. G., Lang, G. A., Dagg, M. J., Whitledge, T. E., & Dortch, Q. (1999). Nutrients, irradiance, and mixing as factors regulating primary production in coastal waters impacted by the Mississippi River plume. *Continental Shelf Research 19*, 1113–1141.

Macedo, M. F., Ferreira, J. G., & Duarte, P. (1998). Dynamic behaviour of photosynthesis-irradiance curves determined from oxygen production during variable incubation periods. *Marine Ecology Progress Series 165*, 31–43.

Martins, M., & Düffner, M. J. (1982). *Estudo da Qualidade da Água. Resultados referentes às observações sinópticas em 1980. Estudo Ambiental do Estuário do Tejo*. Comissão Nacional do Ambiente (CNA)/Tejo N°14-relatório 13. Lisboa (in Portuguese).

Murthy, M. S., Ramakrishna, T., Sarat Babu, G. V., & Rao, Y. N. (1986). Estimation of net primary productivity of intertidal seaweeds—limitations and latent problems. *Aquatic Botany 23*, 383–387.

Muylaert, K., & Sabbe, K. (1999). Spring phytoplankton assemblages in and around the maximum turbidity zone of the estuaries of the Elbe (Germany), the Schelde (Belgium/The Netherlands) and the Gironde (France). *Journal of Marine Systems 22*, 133–149.

NICE (1999). *Nitrogen cycling in estuaries*. Available: http://www.dmu.dk/LakeandEstuarineEcology/NICE.

Partheniades, E. (1965). Erosion and deposition of cohesive soils. *Journal of the Hydraulics Division (ASCE) 91*, 105–139.

Periañez, R., Abril, J. M., & Garcia-Leon, M. (1996). Modelling the suspended matter distribution in an estuarine system. Application to the Odiel River in southwest Spain. *Ecological Modelling 87*, 169–179.

Portela, L. I., & Neves, R. (1994). Numerical modelling of suspended sediment transport in tidal estuaries: a comparison between the Tagus (Portugal) and the Scheldt (Belgium—The Netherlands). *Netherlands Journal of Aquatic Ecology 28*, 329–335.

Quintela, A. (1985). *Hidráulica* (539 pp.). Lisbon: Fundação Calouste Gulbenkian (in Portuguese).

Schild, R., & Prochnow, D. (2001). Coupling of biomass production and sedimentation of suspended sediments in eutrophic rivers. *Ecological Modelling 145*, 263–274.

Serôdio, J., & Catarino, F. (2000). Modelling the primary productivity of intertidal microphytobenthos: time scales of variability and effects of migratory rhythms. *Marine Ecology Progress Series 192*, 13–30.

Simas, T., Nunes, J. P., & Ferreira, J. G. (2001). Effects of global climate change on coastal salt marshes. *Ecological Modelling 139*, 1–15.

Stapleton, C. M., Kay, D., Jackson, G. F., & Wyer, M. D. (2000). Estimated inorganic nutrient inputs to the coastal waters of Jersey from catchment and waste water sources. *Water Research 34*, 787–796.

Valiela, I. (1995). *Marine ecological processes* (2nd ed., p. 43). New York, NY: Springer.

Van Rijn, L. C. (1993). *Principles of sediment transport in rivers, estuaries and coastal seas* (pp. 11–22). Amsterdam: Aqua Publications.

Van Wijngaarden, M. (1999). A two-dimensional model for suspended sediment transport in the southern branch of the Rhine-Meuse estuary, The Netherlands. *Earth Surface Processes and Landforms 24*, 1173–1188.

White, F. M. (1986). *Fluid mechanics* (p. 53). New York, NY: Mc Graw-Hill.